PNAS RESEARCH ARTICLE | EARTH, ATMOSPHERIC, AND PLANETARY SCIENCES

Unexpectedly rapid aerosol formation in the Hunga Tonga plume

Elizabeth Asher[a,b,1,2], Michael Todt[a,b,3], Karen Rosenlof[b], Troy Thornberry[b], Ru-Shan Gao[b], Ghassan Taha[c,d], Paul Walter[e], Sergio Alvarez[f], James Flynn[f], Sean M. Davis[b], Stephanie Evan[g], Jerome Brioude[g], Jean-Marc Metzger[h], Dale F. Hurst[a,i], Emrys Hall[a,i], and Kensy Xiong[a,i]

Edited by Mark Thiemens, University of California San Diego, La Jolla, CA; received November 15, 2022; accepted September 7, 2023

The Hunga Tonga–Hunga Ha'apai (HT-HH) volcanic eruptions on January 13 and 15, 2022, produced a plume with the highest signal in stratospheric aerosol optical depth observed since the eruption of Mt. Pinatubo in 1991. Suites of balloon-borne instruments on a series of launches from Réunion Island intercepted the HT-HH plume between 7 and 10 d of the eruptions, yielding observations of the aerosol number and size distribution and sulfur dioxide (SO_2) and water vapor (H_2O) concentrations. The measurements reveal an unexpected abundance of large particles in the plume, constrain the total sulfur injected to approximately 0.2 Tg, provide information on the altitude of the injection, and indicate that the formation of sulfuric acid aerosol was complete within 3 wk. Large H_2O enhancements contributed as much as ~30% to ambient aerosol surface area and likely accelerated SO_2 oxidation and aerosol formation rates in the plume to approximately three times faster than under normal stratospheric conditions.

stratospheric aerosol | rapid aerosol formation | SO_2 | volcanic plume | Hunga Tonga eruption

Significance

Large volcanic eruptions play an important role in Earth's radiative balance through stratospheric injections of sulfur dioxide that form sulfate aerosol. Here, we show that in situ observations are critical to constrain the injection mass of stratospheric sulfur and the stratospheric lifetime of sulfur dioxide. Such information is needed to better represent aerosol microphysics and improve predictions of the impacts of natural (or potentially anthropogenic) sulfur dioxide injections. Measurements in the fresh volcanic Hunga Tonga–Hunga Ha'apai plume in January 2022 revealed that stratospheric aerosol formation ended approximately three times faster than is typical in the presence of a large amount of water vapor, resulting in a high signal in aerosol extinction from an abundance of large particles.

Volcanic plumes that reach the stratosphere influence Earth's radiative balance and are a significant driver of climate variability (1). Under background conditions, sustaining the stratospheric aerosol burden requires the addition of ~0.1 Tg sulfur (S) y^{-1} from the oxidation of carbonyl sulfide and sulfur dioxide (SO_2) (2), while stratospheric transport (3) and a variety of localized aerosol processes (4) contribute to heterogeneity in aerosol number and size. Simulating an eruption's impact on stratospheric aerosol requires either knowledge or assumptions of its injection height and mass (5), plume composition, location, and atmospheric state. In situ measurements within 1 to 3 wk of an eruption can provide critical information for improving these assumptions.

The energetic eruption of the underwater Hunga Tonga–Hunga Ha'apai (HT-HH) volcano (20.54°S, 175.38°W) on January 15 (04:00 Coordinated Universal Time or UTC) (6), together with a smaller eruption on January 13 (15:20 UTC), injected an estimated 150 Tg water vapor (H_2O) (7) and 0.41 ± 0.01 Tg SO_2 into the stratosphere (7, 8). The combination of its explosivity and the extraordinary amount of H_2O injected into the stratosphere make the January 15 eruption unique in the satellite era. Estimated injection heights for these two eruptions ranged from 20 km on January 13 to >30 km on January 15, and the SO_2 plumes quickly overlapped, making them difficult to distinguish (8). Radiosonde measurements reveal enhanced H_2O between 19 km and the maximum altitude of balloon soundings, near 30 km (9). The HT-HH aerosol layer generated the highest signal in stratospheric aerosol optical extinction since the eruption of Mt. Pinatubo in 1991 (10). The large signal in aerosol extinction sparked questions regarding the initial S injection (11) and the role of H_2O in rapid aerosol formation in this plume and its timeline (12, 13).

In situ observations of particle number concentration and size distribution complement space-based aerosol retrievals. For the first 3 mo after the HT-HH eruption, the Ozone Mapping and Profiler Suite-Limb Profile (OMPS-LP) sensor onboard the Suomi National Polar-orbiting Partnership (S-NPP) satellite supplied a continuous global record of the main volcanic plume's altitude between 16 and 30 km, its horizontal extent and its impact on stratospheric aerosol optical depth (sAOD) (10). The Tonga volcano Rapid Response Experiment (TR^2Ex) provided high-resolution vertical profiles with relatively low uncertainty of SO_2 (14) and H_2O (15, 16) to ~30 km altitude and information on the aerosol size distribution in the main plume, which cannot be reliably inferred from either satellite or ground-based measurements. Here, we leverage a combination of these in situ measurements and OMPS-LP retrievals (17) to address questions regarding the HT-HH eruption's impact on the lifetime of SO_2 and the magnitude and altitude of the initial sulfur injection.

The authors declare no competing interest.

This article is a PNAS Direct Submission.

[1]To whom correspondence may be addressed. Email: elizabeth.asher@noaa.gov.

[2]Present address: National Oceanic and Atmospheric Administration Global Monitoring Laboratory, Boulder, CO, 80305.

[3]Present address: Atmospheric Composition Research, Finnish Meteorological Institute, FI-00101 Helsinki, Finland.

This article contains supporting information online at https://www.pnas.org/lookup/suppl/doi:10.1073/pnas.2219547120/-/DCSupplemental.

Published October 30, 2023.

Results

Rapid Response Insights. TR^{2}Ex was a unique deployment of a suite of balloon-borne instrumentation that repeatedly analyzed the composition of the volcanic plume 7 to 10 d after the second, larger HT-HH eruption. Sampling the fresh HT-HH plume yielded in situ observations of the aerosol size distribution, SO_2, and H_2O at several pivotal times during its evolution (see *Methods, Rapid Response Overview*, for details; *SI Appendix*, Table S1). In situ measurements from this campaign allow us to quantify the S gas/particle phase partitioning within the plume, study the vertical distribution of the S injection, and explore the role of stratospheric H_2O enhancements in increasing ambient aerosol size and extinction.

Portable Optical Particle Spectrometer (POPS) (18) measurements during TR^{2}Ex show the impact of the HT-HH eruption on aerosol dry mass and extinction (enhancements ranged from two to three orders of magnitude), driven by high concentrations of large accumulation mode aerosols in the volcanic plume (Fig. 1; see *Methods, The POPS Measurements and Inherent Assumptions*, for details). By the time the plume reached La Réunion 7 d after the second eruption, wind shear had stretched the initial injection into a thin slanted layer of varying thickness as it moved west (19). Positive altitude gradients in easterly windspeeds resulted in progressively shorter transit times with increasing altitude. TR^{2}Ex instruments were unable to measure two isolated optically thin volcanic aerosol layer segments detected above 30 km by space-based and ground-based remote sensing instruments (10, 19)—as these were above the operation ceiling of balloon sondes. Parts of the aerosol layer between 25 km and 28 km (Fig. 1 *C* and *D*) corresponded to a region with a substantial H_2O enhancement (*SI Appendix*, Fig. S1). Particle number concentration of both large and small particles (up to 1.5 μm) was as much as three orders of magnitude higher than in unperturbed air masses. The mode of the size distribution occurred at ~560 nm diameter, and the aerosol effective radius exceeded 0.3 μm (*SI Appendix*, Fig. S2). With H_2O enhancements of ~340 ppmv in this part of the plume, H_2O contributed ~15% to the aerosol diameter at ~560 nm and ~30% to the total aerosol surface area (*SI Appendix*, Fig. S3; see *Methods, The POPS Measurements and Inherent Assumptions*). Differences in aerosol surface area impact both extinction and stratospheric chemistry (20), highlighting the importance of calculating ambient aerosol size related to the HT-HH eruption. The air was much drier (<17 ppmv H_2O) in the part of the plume below 25 km (*SI Appendix*, Fig. S1), which contained an elevated number concentration of particles <700 nm in diameter (Fig. 1 *E* and *F*). The highest number concentration below 25 km occurred at the smallest particle size, and the aerosol effective radius was not noticeably different from baseline values (~0.2 μm; *SI Appendix*, Fig. S2). Larger particles appeared more often in the wetter, higher altitude parts of the aerosol layer, presumably due to shorter SO_2 lifetimes and particle coagulation within the plume (12).

On three occasions, simultaneous in situ measurements of SO_2 and aerosol in the volcanic plume reveal varying rates of aerosol formation. Particles in the plume are presumed to be composed of sulfuric acid (H_2SO_4) formed from SO_2 oxidation and are designated estimated H_2SO_4 ($_eH_2SO_4$) (see *Methods, The POPS Measurements and Inherent Assumptions*, for details). Comparisons are shown between the mass mixing ratios of S in $_eH_2SO_4$ and SO_2 (Fig. 2 *A–C*). The altitudes of SO_2 enhancements and aerosol accumulations correspond well, and the mass mixing ratios of S in $_eH_2SO_4$ exceeded those of S in SO_2 on two of three flights. Outside of the fresh HT-HH plume, the SO_2 partial pressure was below the detection limit of the SO_2 sonde. If SO_2 gas phase oxidation had proceeded at its typical rate (i.e., an e-folding stratospheric lifetime, τ_{strat} = ~30 d) (22) after the two HT-HH eruptions, we would expect a ≤30% estimated H_2SO_4 ($_eH_2SO_4$) aerosol to ≥70% SO_2 split (by S mass) on January 25, ~10.5 d after the second, larger eruption. In the wetter, higher altitude region of the plume, measured on January 22, $_eH_2SO_4$ aerosol accounted for 90% of the total S in the plume (Fig. 2*D*), implying a τ_{strat} = ~3 d. In a drier part of the aerosol layer encountered on January 24 at 22 km, $_eH_2SO_4$ aerosol constituted 68% of the total S (τ_{strat} = ~8 d), and on January 25 at 20 km, only 35% of the total S (τ_{strat} = ~24 d). We infer that SO_2 oxidation in the fresh plume proceeded at different rates as a function of H_2O, namely more quickly where H_2O mixing ratios were higher due to an increased concentration of hydroxyl radicals (23, 24). These measurements also provide information on the vertical distribution of the S injection (i.e., the sum of the S in both SO_2 and in $_eH_2SO_4$ aerosol; Fig. 2*D*). The total S column mass of the higher altitude part of the plume measured on January 22 was nearly four times that of the lower altitude part of the plume measured on January 24 and January 25, suggesting that the majority of SO_2 was injected above 25 km (Fig. 2*D*).

Aerosol Burden and Stratospheric Lifetime of SO_2. Quantifying the S burden in the plume helps constrain the stratospheric S injection and the stratospheric lifetime (τ_{strat}) of SO_2, which are critical for model validation and have widespread implications for stratospheric chemistry. The calculation relies on the relationship between the aerosol S column and sAOD calculated using POPS size distributions on launches from La Réunion and on OMPS-LP

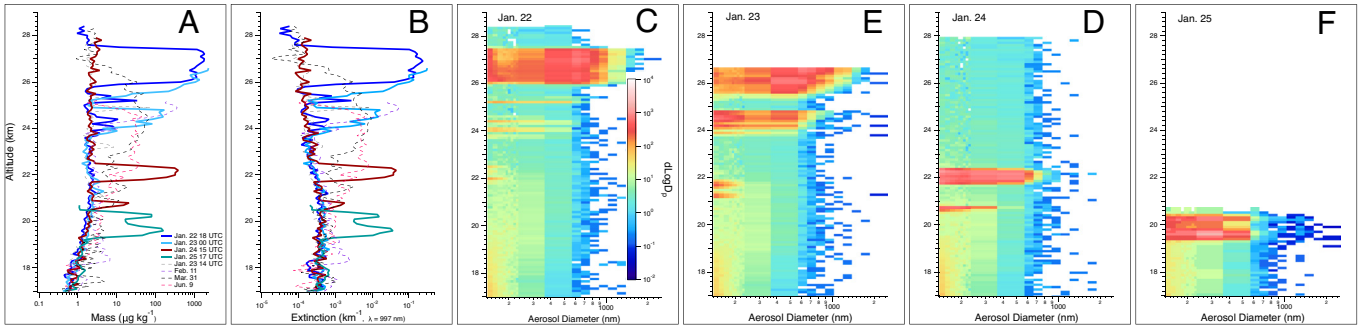

Fig. 1. Vertical profiles of calculated bulk aerosol properties between January and June 2022 (from POPS size distribution data), including mass mixing ratios (*A*) and ambient extinction using Steele and Hamill (21) (*B*), both of which use the legend in panel (*A*), and vertical profiles of the measured aerosol size distributions from TR^{2}Ex launches when the fresh HT-HH aerosol plume was encountered (*C–F*). Aerosol size distributions (dN/dLogD$_p$) for the four TR^{2}Ex soundings (*C–F*) use the color scale in panel (*C*).

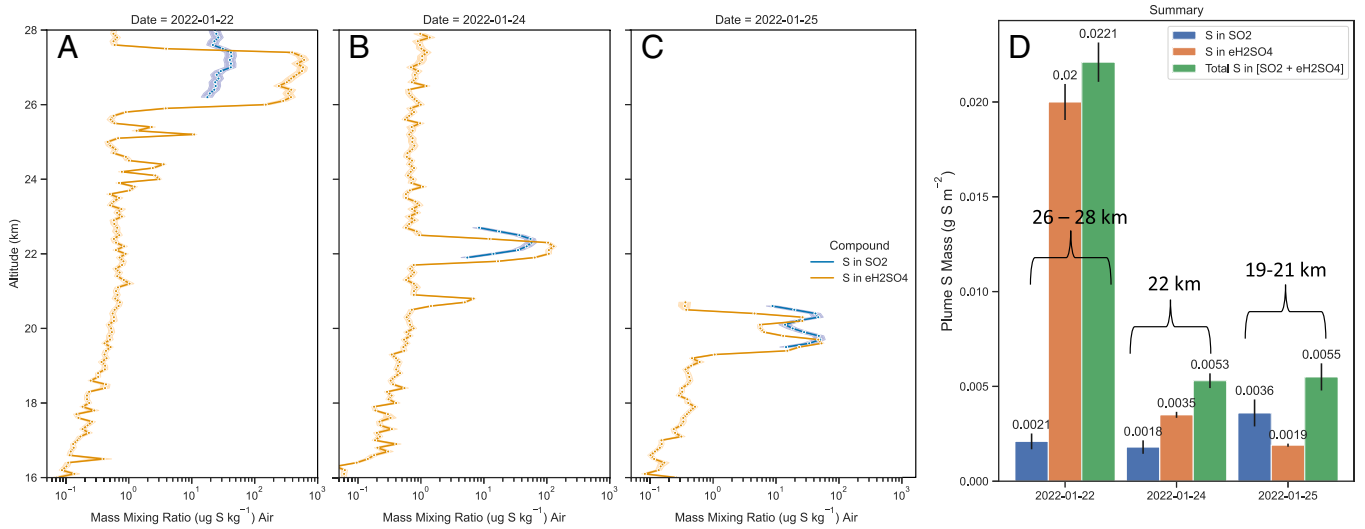

Fig. 2. Vertical profiles of the mass mixing ratios of S in SO_2 and of S in $_eH_2SO_4$ calculated based on aerosol size distributions, when both instruments measured the volcanic plume with low uncertainties (*A*–*C*), and a summary of the S column mass in SO_2, the S column mass in $_eH_2SO_4$, and the total S column mass ([S in SO2] + [S in $_eH_2SO_4$] observed within the plume (*D*). Shaded areas and error bars show the uncertainty in SO_2 sonde measurements (≤20%) and the uncertainty in calculated eH_2SO_4 including possible error related to aerosol sizing and aerosol density.

retrievals of sAOD (*Methods, Calculating the Aerosol Column and Plume S Burden*). As the plume moved westward, TR^{2}Ex launches sampled its core on January 22 to 23 and trailing edge on January 24 to 25 (Fig. 3). The S in the $_eH_2SO_4$ aerosol layer grew from 0.03 Tg S on January 18 to 0.14 Tg S on January 26 and reached a maximum of 0.18 Tg S on February 3 (Fig. 4*A*). We estimate that on January 23, ~3/4 of the S mass was located in the higher altitude part of the aerosol layer, west of La Réunion (Fig. 4*A*; *Methods, Calculating the AerosolColumn and Plume S Burden*). Leading up to the eruptions (i.e., on January 10), the S burden in background $_eH_2SO_4$ aerosol was < 0.001 Tg S. This result suggests that rapid aerosol conversion took place: Within ~19 d, as much as 0.18 Tg S SO_2 released from the eruptions (8) was oxidized and converted to particles (≥140 nm). By tracking the accumulation of S in $_eH_2SO_4$ aerosol, we calculate the average τ_{strat} as ~10 to 14 d in the plume (see *Methods, Estimating the SO_2 Lifetime*; Fig. 4*B*). We note, however, that if a sizeable fraction (e.g., 0.09 Tg) of the aerosol mass were not composed of H_2SO_4, this would yield a longer estimated τ_{strat} (~15 to 18 d) given the same SO_2 injection. A short τ_{strat}, compared with the typical value of 1 mo under climatological stratospheric conditions, helps explain the rapid production of large particles in the HT-HH plume and signals greater availability of the hydroxyl radical to react with methane and trace gases in the stratosphere (12, 23, 24).

Discussion

A rapid response to large or unusual volcanic eruptions with in situ observations can provide insight into the resulting aerosol microphysics, complement space-based aerosol retrievals (7, 8, 10), and be essential to evaluate models. Together with satellite retrievals of sAOD, POPS vertical profiles of particle size distributions enable the calculation of the aerosol layer's S mass and the mean τ_{strat} of SO_2. We determined that $_eH_2SO_4$ formation was complete within 3 wk, which is consistent with a maximum effective radius (>0.4 μm) observed in early February (*SI Appendix*, Fig. S2). In situ measurements of SO_2 and $_eH_2SO_4$ and calculations of the aerosol layer's S mass provide evidence that the bulk of the total S was injected above 25 km, which cannot be easily deduced from satellite retrievals of SO_2 and aerosol extinction (8, 10). These observations also indicate that SO_2 oxidation and aerosol conversion occurred at varying rates within the plume, corresponding to localized H_2O enhancements. Radiosonde measurements confirm that H_2O mixing ratios within the plume spanned more than an order of magnitude (<100 ppmv to >1,000 ppmv) (9). Climatological lower stratospheric mixing ratios in the tropics do not typically exceed 4 to 5 ppmv (25). SO_2 oxidation and aerosol conversion took place approximately three times faster, on average, than under climatological stratospheric conditions. SO_2 oxidation accelerates substantially in the presence of H_2O enhancements (12, 23, 24, 26). A short τ_{strat} of SO_2 reflects the heightened oxidative capacity of the atmosphere, with important implications for stratospheric chemistry and composition.

Our measurements clarify the contributions to aerosol extinction from H_2O after the HT-HH eruptions, which has spurred discussion in the scientific community (10–13). We caution against conflating a response in the aerosol extinction with a similar change in aerosol mass for two reasons: H_2O contributed ~30% to aerosol extinction in the fresh HT-HH plume, and light scattering efficiency is closely related to aerosol size, with a maximum efficiency (per unit volume) at 500 nm diameter (20). Due to the 560 nm diameter mode of the measured aerosol size distribution mode and large H_2O enhancements, the HT-HH aerosol layer resulted in a high sAOD relative to its injected mass. Radiosonde measurements show elevated H_2O throughout the plume between January 20 and February 1 (one-quarter of the observations between 26 and 28 km altitude from all vertical profiles during this period had $7 \leq H_2O \leq 130$ ppmv) (27), signifying widespread implications for $_eH_2SO_4$ particle size and the S mass in the higher altitude part of the aerosol layer. Particle size distributions show that differences in the peak and shape of the size distribution result in substantial differences in aerosol extinction (e.g., Fig. 1). Questions remain about how H_2O and other compounds reaching the stratosphere during an eruption might influence aerosol microphysics, including the propensity for new particle formation, condensation onto existing particles, and particle coagulation.

TR^{2}Ex serves as a roadmap for future rapid response campaigns to volcanic eruptions and other stratospheric perturbations. Campaigns such as TR^{2}Ex further the understanding of

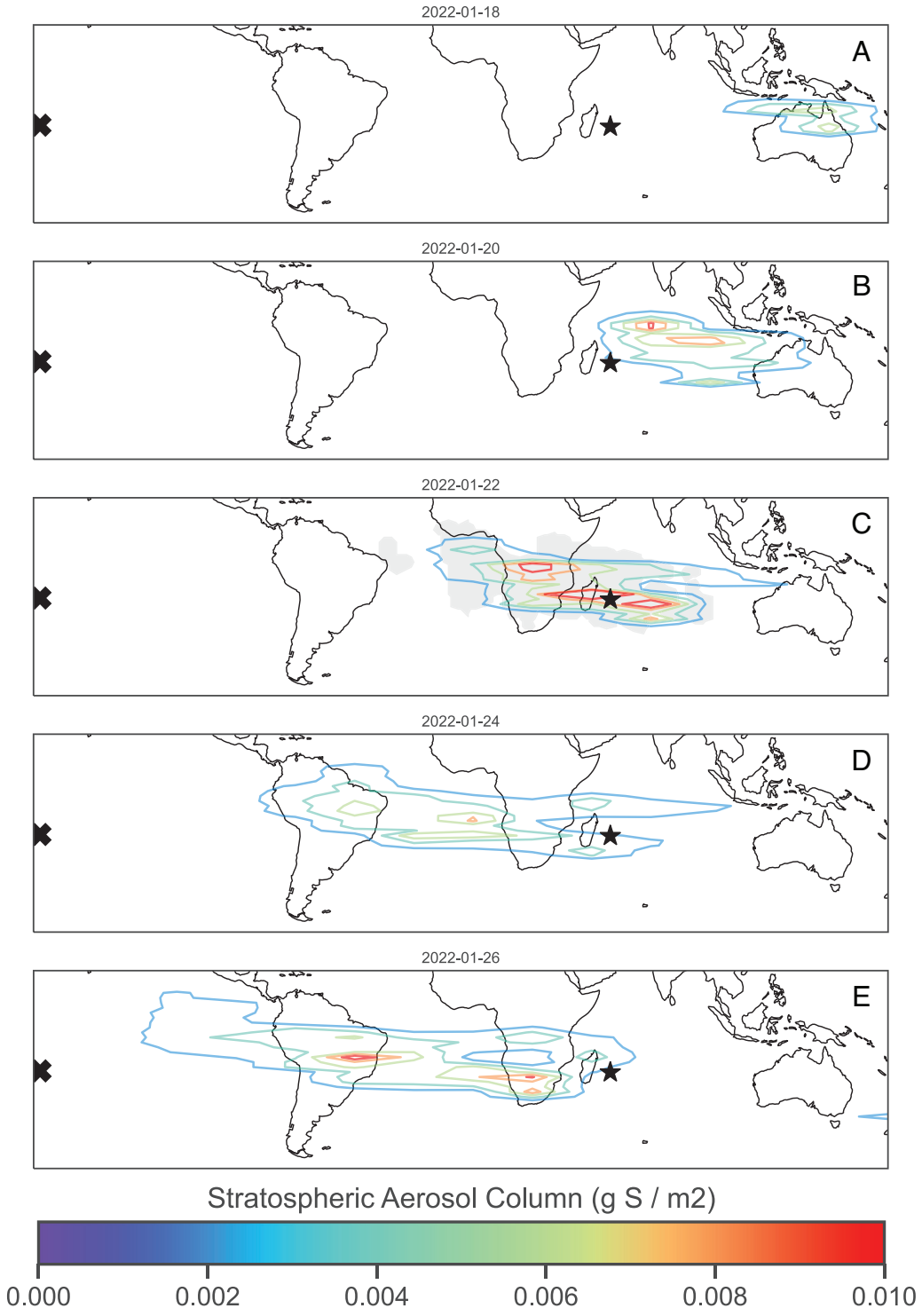

Fig. 3. Contour plots of the S in $_eH_2SO_4$ column (g m^{-2}), calculated using the equation in the *SI Appendix*, Fig. S4*A* caption, for 5 d from January 18 to January 26 (*A*–*E*). On January 22, the gray shaded area shows the maximum H_2O plume extent between January 21 and January 23 as determined from MLS H_2O anomalies at 21 hPa. Locations of HT-HH and La Réunion are marked with a cross and star, respectively.

aerosol processes in the stratosphere and inform models predicting climate impacts under a variety of past and potential future conditions. Stratospheric aerosol injection (SAI), one proposed method of climate intervention, would entail a large anthropogenic addition of stratospheric aerosol. The suite of instruments described here is capable of identifying potential SAI implementations, providing insight into the aerosol composition (i.e., sulfate or other) and could enable quantifying the mass (and altitude) of SAI.

Methods

Rapid Response Overview. POPS in situ observations (18) of aerosol size distributions were made as part of the National Oceanic and Atmospheric Administration (NOAA) Earth Radiation Budget program's Baseline Balloon Stratospheric Aerosol Profiles (B^2SAP) project (28). The B^2SAP project combines intensive periods of operation (IOP) with routine baseline measurements in the northern and southern hemispheres. For TR^2Ex between January 21 and January 26, B^2SAP IOP activities were coordinated with additional sonde and lidar

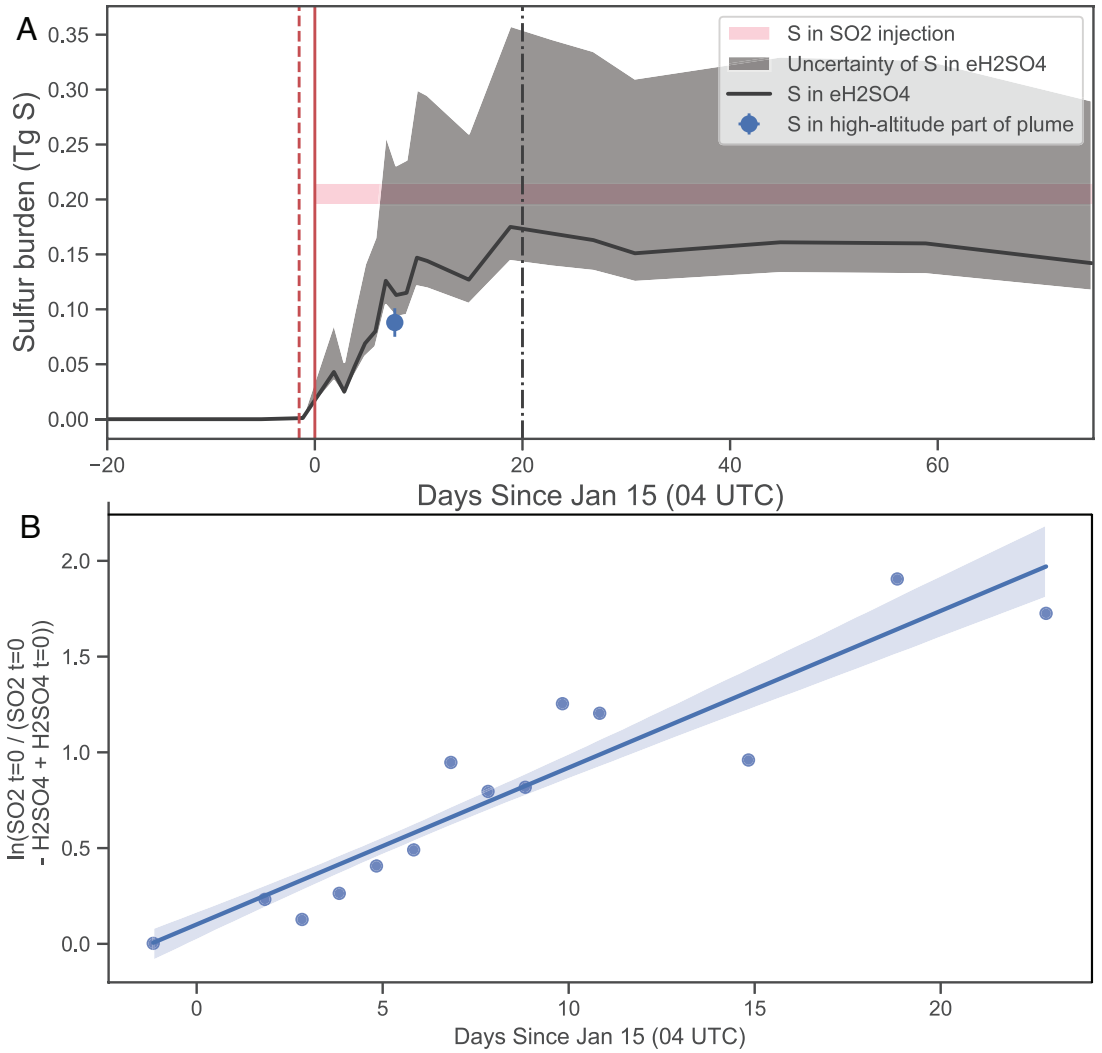

Fig. 4. A time series of the S burden in ${}_eH_2SO_4$ aerosol, calculated using a combination of POPS measurements and OMPS-LP retrievals (*A*) and the estimation of the τ_{strat} (*B*). The S burden in ${}_eH_2SO_4$ aerosol (black line) represents the relationship between calculated ambient sAOD and the mass and agrees with estimates of the S injected as SO_2 from satellites (7, 8) (pink shaded region). The uncertainty (black shaded region) represents the range of assumptions considered in *SI Appendix*, Fig. S4*A*. The approximated S mass in the higher altitude part of the plume, west of La Réunion on January 23 00 UTC, is also shown. OMPS-LP dashed vertical lines depict the period of ${}_eH_2SO_4$ aerosol accumulation. The S burden from this period is used to calculate the stratospheric lifetime of SO_2, τ_{strat} = 1/k, as shown in Eq. **2** (*Methods, Calculating the Aerosol Column and Plume S Burden*). Assuming an SO_2 injection of 0.205 Tg S in SO_2 (7, 8) k = 0.08 (r^2 = 0.87; P < 1.30E-6; 1 SD of the slope is ±0.009), suggesting a τ_{strat} for SO_2 of ~12 d (*B*).

measurements at the Maïdo Observatory (19) on La Réunion (21°S, 55°E). TR^2Ex balloon payloads consisted of either: (A) a POPS, a sulfur dioxide (SO_2) sonde, an Electrochemical Concentration Cell (ECC) ozonesonde and a radiosonde, or (B), an ECC ozonesonde, a Compact Optical Backscatter Aerosol Detector (COBALD) instrument and a radiosonde (*SI Appendix*, Table S1; COBALD, ozonesonde, and lidar measurements are discussed elsewhere (19). The ground-based lidars and the COBALD provided information on aerosol extinction (19) and backscattering, respectively. Unfortunately, quantitative information on the aerosol depolarization in the plume during TR^2Ex does not exist because the lidar at the Maïdo observatory was not calibrated for depolarization. Subsequent POPS and NOAA Frost point Hygrometer (FPH) launches in February, March, and June 2022 at the Maïdo Observatory were part of what are now routine B^2SAP soundings (*SI Appendix*, Table S1) (28).

SO_2 sonde (14) measurements have lower uncertainty and considerably better vertical resolution than satellite SO_2 retrievals (8), particularly after an energetic volcanic eruption. A modified ECC ozonesonde, the SO_2 sonde removes ozone from the sample prior to detection using a filter, allowing stratospheric as well as tropospheric SO_2 to be quantified using preflight calibrations (14). The SO_2 sonde has a ~25 s response time, similar to that of an ozonesonde. SO_2 data (Fig. 2) reflect a correction for this time (and altitude) lag (29, 30). CFH (31) and FPH (16) instruments measuring H_2O were used to calculate ambient particle size, and Ozone Mapping and Profiler Suite-Limb Profile (OMPS-LP) retrievals (17) were used to calculate the volcanic plume's aerosol burden, as described below.

The POPS Measurements and Inherent Assumptions. Particle sizing inherently requires assumptions about particle morphology and refractive index related to aerosol composition (18). Here, we assume that particles are spherical and composed of sulfuric acid (H_2SO_4) and water, with a corresponding refractive index of 1.45 at 405 nm (the wavelength of the POPS laser), leading to a reported particle number and size distribution between 140 nm and 2.5 μm in diameter. Telemetered data are quality assured based on available engineering parameters, including the instrument temperature, measured with a thermistor located on the POPS laminar flow element, and the instrument flow (28). Particles are expected to be at (or close to) equilibrium with the instrument temperature at the time of detection, given a particle transit time of 60 to 90 ms. We note that POPS particle transit times exceeded modeled timescales required for aerosol growth or evaporation that could occur during sampling, in line with similar calculations from Kovilakam and Deshler (32) and Jonsson et al. (33).

The S in the ${}_eH_2SO_4$ aerosol column mass and mass mixing ratios are calculated from the measured aerosol size distribution and particle density. The aerosol weight (wt.%) ${}_eH_2SO_4$ can be determined using the partial pressure of H_2O at a range of temperatures (21, 34–36). We apply the formulation of Tabazedah et al.

(36), which is suitable for low temperatures observed in the lower stratosphere (when ${}_eH_2SO_4 \leq 80$ wt. %) and is based on Steele and Hamill (21), and the expression of Gmitro and Vermeulen when ${}_eH_2SO_4 > 80$ wt. % (34). In the stratosphere, particles have a calculated ≥80% wt% ${}_eH_2SO_4$ at the time of detection due to instrument temperatures (268 to 278 K) that are considerably higher than ambient stratospheric air ($\Delta T = 50$ to 75 K). Particle density at the time of detection is both wt.% and temperature dependent (37, 38). We use two parameterizations valid for temperatures between 233 and 298 K given different wt. % (37, 38).

Ambient particle diameter is calculated according to Steele and Hamill (21) from the measured (dehydrated) particle diameter, the particle wt. %, and density both at the time of detection and in ambient air, assuming that the particle was at equilibrium in both cases and that only water (not H_2SO_4) was lost from the particle during sampling (*SI Appendix*, Fig. S3*A*). Measured aerosol size distributions were averaged into 100 m altitude bins to improve counting statistics and facilitate the requisite merges with frost point hygrometer data from other launches. Possible errors in measured particle sizing are driven primarily by Mie resonances (18). Uncertainty in H_2O (≤6%), air temperature (<1%), and uncertainties in the parameterizations of the wt. % and density contribute additionally to possible errors in calculated ambient sizing (*SI Appendix*, Fig. S3), and the mass mixing ratios and column mass of S in ${}_eH_2SO_4$ (Fig. 2).

As in situ size distribution measurements provide no information on aerosol composition, we cannot rule out the possibility that aerosol could have consisted of ash or some other material, such as sea salt, coated (or internally mixed) with H_2SO_4. Contributions from HNO_3 aerosol or mixtures containing HNO_3 and H_2SO_4 were considered but dismissed based on equilibrium calculations (39, 40). Although volcanic lightning on January 15 (41) may have injected NO directly into the stratosphere, HNO_3 hardly condenses at temperatures ≥220 K observed in the plume, despite large enhancements in stratospheric H_2O.

The assumptions made here regarding particle composition and morphology are supported by space-based Cloud-Aerosol Lidar with Orthogonal Polarization (CALIOP) retrievals and geostationary satellite RGB-Ash composite imagery within the first few days of the HT-HH eruption on January 15 (11). CALIOP retrievals showed particles with low depolarization, indicating spherical H_2SO_4 particles moving westward toward La Réunion on January 20. The geostationary satellite RGB-Ash composite images depicted a concomitant light green SO_2 plume (with little to no ash) during this period.

Calculating the Aerosol Column and Plume S Burden. Vertical profiles of aerosol extinction at 997 nm, corresponding to the native wavelength of the OMPS-LP sensor, are calculated using publicly available Mie codes (42, 43) and the calculated particle size distribution in ambient air. POPS stratospheric ambient aerosol optical depth (sAOD) is the sum of calculated ambient aerosol extinction above the tropopause. Similarly, the POPS stratospheric S column in ${}_eH_2SO_4$ aerosol (g S m^{-2}) at a single geographic location is quantified as the sum of the S in ${}_eH_2SO_4$ aerosol (μg S m^{-2} air) in each 100 m altitude bin above the tropopause. A baseline value of the S column in ${}_eH_2SO_4$ aerosol, calculated from a vertical profile outside the plume on January 23 (14 UTC), was subtracted from each measurement that encountered the plume to determine the S in the aerosol layer (g S m^{-2}). Because SO_2 measurements were below the SO_2 sonde's limit of detection outside the plume, no similar subtraction of the S column in SO_2 under baseline conditions was made for comparisons in Fig. 2*D*.

A linear regression between the POPS calculated ambient sAOD and the stratospheric S in ${}_eH_2SO_4$ column enables global retrievals of OMPS-LP sAOD to be used to infer the S in ${}_eH_2SO_4$ column mass across the entire aerosol layer and to track the S aerosol burden as the plume evolves. Relationships between the sAOD based on POPS measured particle size distributions as well as sAOD based on the calculated ambient particle size distributions and the POPS S in ${}_eH_2SO_4$ column (±uncertainty) over La Réunion between January 22 and June 9 are shown in *SI Appendix*, Fig. S4*A*. The reported uncertainty in OMPS-LP sAOD signal in the stratosphere (10% at λ = 997 nm) (17) is negligeable compared to the differences in the slope and intercept of the POPS sAOD vs. mass relationships (*SI Appendix*, Fig. S4*A*). We note that recent debate with respect to potential OMPS-LP retrieval biases (44) is beyond the scope of this work but would lead to a lower ${}_eH_2SO_4$ aerosol layer mass. The maximum value of daily sAOD from the OMPS-LP sensor on January 10 (50°S–50°N) was used as the sAOD threshold to identify the geographic extent of the tropical HT-HH aerosol layer (*SI Appendix*, Fig. S4*B*); its median (0.0025) was used as a background sAOD value in the tropics. The linear relationships from *SI Appendix*, Fig. S4*A* were applied to each daily sAOD value in the aerosol layer to infer the S column (g S m^{-2}) in each (2° latitude × 24° longitude) grid cell. The resulting S column using the relationship between the ambient sAOD and S in ${}_eH_2SO_4$ column mass is shown in Fig. 3. For reference, the H_2O plume extent, calculated from MLS retrieval levels between 10 and 46 hPa using MLS H_2O anomalies between January 21 and January 23 (defined as the median ± 3× the mean absolute deviation), is also shown in Fig. 3*C*, compared to the aerosol layer.

The S column was then multiplied by the area of the corresponding geographic grid cell (m^2) and summed to determine the total stratospheric S burden (Tg S) over that area. By applying the relationships from *SI Appendix*, Fig. S4*A* to the background sAOD value, multiplied by the aerosol layer's geographic area, we similarly calculated the corresponding S burden under background conditions in each case. The S burden under background conditions was then subtracted from the total stratospheric aerosol S burden to yield the volcanic aerosol layer's S burden (Tg S) shown in Fig. 4. The uncertainty in the S burden (the shaded black region) reflects the range of the estimates shown in *SI Appendix*, Fig. S4*A*. The S mass in the upper part of the plume was approximated as the sum of the S burden (in ${}_eH_2SO_4$ aerosol) west of La Réunion (55°E), when the higher altitude part of the aerosol layer was last observed on January 23 00 UTC (Fig. 1*D*) (19). La Réunion is located near the latitudinal edge (48°E) of two adjacent OMPS-LP grid cells. Thus, this estimate represents the arithmetic mean (±the SD) of the S burden in the adjacent OMPS-LP grid cells centered at 36°E and 60°E (Fig. 4).

Estimating the SO_2 Lifetime. By monitoring the aerosol loading following an eruption, we can estimate the initial injection of S and subsequently deduce the stratospheric lifetime (τ_{strat}) of SO_2. We assume that all the SO_2 is converted to H_2SO_4:

$$\frac{d[H_2SO_4]}{dt} = -\frac{d[SO_2]}{dt}, \text{ and } [SO_{2_t}] = [SO_{2_{t=0}}] - ([H_2SO_{4_t}] - [H_2SO_{4_{t=0}}]). \quad [1]$$

Making these substitutions into the first-order rate law $\frac{d[SO_2]}{[SO_2]} = -kdt$ and integrating demonstrates that the calculated rate of H_2SO_4 production is influenced by the initial injection of SO_2 and by the background H_2SO_4 burden (together with any initial injection of aerosol). We calculate the τ_{strat} of SO_2 through linear regression against t (elapsed days since 4:00 UTC on January 15), where k is the slope of the line and $\tau_{strat} = 1/k$:

$$ln\frac{[SO_{2_{t=0}}]}{[SO_{2_{t=0}}] - ([H_2SO_{4_t}] - [H_2SO_{4_{t=0}}])} = kt. \quad [2]$$

The initial injection of S, $SO_{2t=0}$, is based on satellite retrievals of SO_2, which are slightly greater than the maximum accrual of S in ${}_eH_2SO_4$ aerosol after the eruption (0.18 Tg; Fig. 4*A*). τ_{strat} was calculated using a range of values for the initial SO_2 injection (0.195 to 0.215 Tg S in SO_2) (7, 8). Prior to the eruption (e.g., on January 10), the initial S burden in the aerosol layer is close to zero (0.0005 Tg S in ${}_eH_2SO_4$), which is used as the value for $H_2SO_{4_{t=0}}$. If as much as 0.09 Tg of aerosol mass were not composed of H_2SO_4 (0.03 Tg S is in 0.09 Tg ${}_eH_2SO_4$) this would result in an estimated τ_{strat} of 15 to 18 d. Eq. **2** ignores a potential time lag required for either particle formation or aerosol growth through condensation to particle diameter ≥0.14 μm from H_2SO_4 gas, considered negligible in this case.

Data, Materials, and Software Availability. The processed POPS aerosol size distribution data from all launches used in this study may be found under the supporting data tab for this manuscript at https://csl.noaa.gov/projects/b2sap/data.html (45) where processed SO_2 and H_2O data from TR^2Ex, and processed daily files of OMPS-LP sAOD and MLS H_2O plume areas and anomalies from 21 hPa are also available. Raw OMPS-LP and MLS H2O data may be found at https://disc.gsfc.nasa.gov/datasets/OMPS_NPP_LP_L2_AER_DAILY_2/summary (46) and https://disc.gsfc.nasa.gov/datasets/ML2H2O_004/summary?keywords=aura (47), respectively. Code is publicly available at https://github.com/elizabethasher/hthhPY (48).

ACKNOWLEDGMENTS. This work was supported by the National Oceanic and Atmospheric Administration (NOAA) Earth Radiation Budget program. We acknowledge the European Communities, the Région Réunion, CNRS, and Université de la Réunion for their support and contributions in the construction phase of the research infrastructure OPAR (Observatoire de Physique de l'Atmosphère de La Réunion, including Maïdo Observatory). OPAR is presently funded by CNRS (INSU), Météo France, and Université de La Réunion and managed by OSU-R (Observatoire des Sciences de l'Univers de La Réunion, UAR 3365). Development, maintenance, and analysis of the OMPS-LP aerosol product are supported by the NASA Earth Science TASNPP (grant # 80NSSC18K0847) and SNPPSP (grant # 80NSSC22K0157) programs. Opinions, findings, and conclusions contained herein reflect the authors' views, not those of NOAA.

Author affiliations: [a]Cooperative Institute for Research in Environmental Sciences, University of Colorado Boulder, Boulder, CO 80309; [b]National Oceanic and Atmospheric Administration Chemical Sciences Laboratory, Boulder, CO 80305; [c]Morgan State University, Baltimore, MD 21251; [d]NASA Goddard Space Flight Center, Greenbelt, MD 20771; [e]Department of Mathematics, St. Edward's University, Austin, TX 78704; [f]Department of Earth and Atmospheric Sciences, University of Houston, Houston, TX 77004; [g]Laboratoire de l'Atmosphère et des Cyclones, UMR8105, CNRS, Université de La Réunion, Saint-Denis 97744, France; [h]Observatoire des Sciences de l'Univers de la Réunion, Unité d'Appui et de Recherche 3365 (CNRS, Université de la Réunion, Météo-France), Saint-Denis 97744, France; and [i]National Oceanic and Atmospheric Administration Global Monitoring Laboratory, Boulder, CO 80305

Author contributions: E.A., K.R., T.T., and R.-S.G. designed research; E.A., M.T., P.W., S.A., S.E., J.B., and J.-M.M. performed research; E.A., R.-S.G., J.F., S.A., P.W., D.F.H., E.H., K.X., J.B., and S.E. contributed new reagents/analytic tools; E.A., M.T., G.T., P.W., S.M.D., S.E., and E.H. analyzed data; K.R., S.E., and T.T. helped organize the filed campaign; K.R., T.T., P.W., R.-S.G., and S.M.D. provided feedback on analysis and ideas and writing; S.M.D. provided Microwave Limb Sounder H_2O data and analysis for this study; G.T. provided the Ozone Mapping and Profiler Suite-Limb Profile data for this study; and E.A. wrote the paper.

1. S. Solomon *et al.*, The persistently variable "background" stratospheric aerosol layer and global climate change. *Science* **333**, 866–870 (2011).
2. A. Feinberg *et al.*, Improved tropospheric and stratospheric sulfur cycle in the aerosol–chemistry–climate model SOCOL-AERv2. *Geosci. Model Dev.* **12**, 3863–3887 (2019).
3. M. H. Hitchman, M. McKay, C. R. Trepte, A climatology of stratospheric aerosol. *J. Geophys. Res.* **99**, 20689 (1994).
4. S. Kremser *et al.*, Stratospheric aerosol-observations, processes, and impact on climate: Stratospheric aerosol. *Rev. Geophys.* **54**, 278–335 (2016).
5. L. O. Muser *et al.*, Particle aging and aerosol–radiation interaction affect volcanic plume dispersion: Evidence from the Raikoke 2019 eruption. *Atmos. Chem. Phys.* **20**, 15015–15036 (2020).
6. C. J. Wright *et al.*, Surface-to-space atmospheric waves from Hunga Tonga-Hunga Ha'apai eruption. *Nature* **609**, 741–746 (2022).
7. L. Millán *et al.*, The Hunga Tonga-Hunga Ha'apai hydration of the stratosphere. *Geophys. Res. Lett.* **49**, e2022GL099381 (2022).
8. S. A. Carn, N. A. Krotkov, B. L. Fisher, C. Li, Out of the blue: Volcanic SO2 emissions during the 2021–2022 eruptions of Hunga Tonga–Hunga Ha'apai (Tonga). *Front. Earth Sci.* **10**, 976962 (2022).
9. H. Vömel, S. Evan, M. Tully, Water vapor injection into the stratosphere by Hunga Tonga-Hunga Ha'apai. *Science* **377**, 1444–1447 (2022).
10. G. Taha *et al.*, Tracking the 2022 Hunga Tonga-Hunga Ha'apai aerosol cloud in the upper and middle stratosphere using space-based observations. *Geophys. Res. Lett.* **49**, e2022GL100091 (2022), 10.1029/2022GL100091.
11. B. Legras *et al.*, The evolution and dynamics of the Hunga Tonga-Hunga Ha'apai sulfate aerosol plume in the stratosphere. *Atmos. Chem. Phys.* **22**, 14957–14970 (2022).
12. Y. Zhu *et al.*, Perturbations in stratospheric aerosol evolution due to the water-rich plume of the 2022 Hunga-Tonga eruption. *Commun. Earth Environ.* **3**, 248 (2022).
13. M. R. Schoeberl *et al.*, Analysis and impact of the Hunga Tonga-Hunga Ha'apai stratospheric water vapor plume. *Geophys. Res. Lett.* **49**, e2022GL100248 (2022).
14. S. Yoon *et al.*, Development and testing of a novel sulfur dioxide sonde. *Atmos. Meas. Tech.* **15**, 4373–4384 (2022).
15. H. Vömel, T. Naebert, R. Dirksen, M. Sommer, An update on the uncertainties of water vapor measurements using cryogenicfrost point hygrometers. *Atmos. Meas. Tech.* **9**, 3755–3768 (2016).
16. E. G. Hall *et al.*, Advancements, measurement uncertainties, and recent comparisons of the NOAAfrost point hygrometer. *Atmos. Meas. Tech.* **9**, 4295–4310 (2016).
17. G. Taha *et al.*, OMPS LP Version 2.0 multi-wavelength aerosol extinction coefficient retrieval algorithm. *Atmos. Meas. Tech.* **14**, 1015–1036 (2021).
18. R. S. Gao *et al.*, A light-weight, high-sensitivity particle spectrometer for PM2.5 aerosol measurements. *Aerosol Sci. Technol.* **50**, 88–99 (2016).
19. A. Baron *et al.*, Early evolution of the stratospheric aerosol plume following the 2022 Hunga Tonga-Hunga Ha'apai Eruption: Lidar observations from reunion (21°S, 55°E). *Geophys. Res. Lett.* **50**, e2022GL101751 (2023).
20. D. M. Murphy *et al.*, Radiative and chemical implications of the size and composition of aerosol particles in the existing or modified global stratosphere. *Atmos. Chem. Phys.* **21**, 8915–8932 (2021).
21. H. M. Steele, P. Hamill, Effects of temperature and humidity on the growth and optical properties of sulphuric acid–water droplets in the stratosphere. *J. Aerosol Sci.* **12**, 517–528 (1981).
22. M. Höpfner *et al.*, Sulfur dioxide (SO2) from MIPAS in the upper troposphere and lower stratosphere 2002–2012. *Atmos. Chem. Phys.* **15**, 7017–7037 (2015).
23. A. N. LeGrande, K. Tsigaridis, S. E. Bauer, Role of atmospheric chemistry in the climate impacts of stratospheric volcanic injections. *Nat. Geosci.* **9**, 652–655 (2016).
24. J. H. Seinfeld, S. N. Pandis, *Atmospheric Chemistry and Physics: From Air Pollution to Climate Change* (John Wiley & Sons, 2006).
25. D. F. Hurst *et al.*, Recent divergences in stratospheric water vapor measurements by frost pointhygrometers and the Aura Microwave Limb Sounder. *Atmos. Meas. Tech.* **9**, 4447–4457 (2016).
26. Y. Zhu *et al.*, Persisting volcanic ash particles impact stratospheric SO2 lifetime and aerosol optical properties. *Nat. Commun.* **11**, 4526 (2020).
27. H. Vömel, Hunga Tonga-Hunga Ha'apai stratospheric water vapor from Vaisala RS41 radiosondes [dataset]. UCAR/NCAR - GDEX. https://doi.org/10.5065/P328-Z959. Accessed 25 September 2022.
28. M. A. Todt *et al.*, Baseline balloon stratospheric aerosol profiles (B^2 SAP)-Systematic measurements of aerosol number density and size. *J. Geophys. Res. Atmos.* **128**, e2022JD038041 (2023).
29. H. Vömel *et al.*, A new method to correct the electrochemical concentration cell (ECC) ozonesonde time response and its implications for "background current" and pump efficiency. *Atmos. Meas. Tech.* **13**, 5667–5680 (2020).
30. L.-J. Huang, M.-J. Chen, C.-H. Lai, H.-T. Hsu, C.-H. Lin, New data processing equation to improve the response time of an electrochemical concentration cell (ECC) ozonesonde. *Aerosol Air Qual. Res.* **15**, 935–944 (2015).
31. H. Vömel, D. E. David, K. Smith, Accuracy of tropospheric and stratospheric water vapor measurements by the cryogenic frost point hygrometer: Instrumental details and observations. *J. Geophys. Res.* **112**, D08305 (2007).
32. M. Kovilakam, T. Deshler, On the accuracy of stratospheric aerosol extinction derived from in situ size distribution measurements and surface area density derived from remote SAGE II and HALOE extinction measurements. *J. Geophys. Res. Atmos.* **120**, 8426–8447 (2015).
33. H. H. Jonsson *et al.*, Performance of a focused cavity aerosol spectrometer for measurements in the stratosphere of particle size in the 0.06–2.0-μm-diameter range. *J. Atmos. Ocean Technol.* **12**, 115–129 (1995).
34. J. I. Gmitro, T. Vermeulen, Vapor–liquid equilibria for aqueous sulfuric acid. *AIChE J.* **10**, 740–746 (1964).
35. S. L. Clegg, P. Brimblecombe, Application of a multicomponent thermodynamic model to activities and thermal properties of 0–40 mol kg^{-1} aqueous sulfuric acid from <200 to 328 K. *J. Chem. Eng. Data* **41**, 1530–1530 (1996).
36. A. Tabazadeh, O. B. Toon, S. L. Clegg, P. Hamill, A new parameterization of H_2SO_4/H_2O aerosol composition: Atmospheric implications. *Geophys. Res. Lett.* **24**, 1931–1934 (1997).
37. E. W. Washburn, Ed., *International Critical Tables of Numerical Data, Physics, Chemistry and Technology* (McGraw-Hill, 1928).
38. L. Oca, J. M. Campillo-Robles, M. M. Bou-Ali, Review and analysis of thermophysical properties of a sulfuric acid-water electrolyte. *J. Chem. Eng. Data* **63**, 3572–3583 (2018).
39. J. A. Goff, S. Gratch, "Low-pressure properties of water from -160 to 212 °F" in *Transactions of the American Society of Heating and Ventilating Engineers* (Transactions of the American Society of Heating and Ventilating Engineers, 1946), pp. 95–122.
40. M. D. Petters, S. M. Kreidenweis, A single parameter representation of hygroscopic growth and cloud condensation nucleus activity. *Atmos. Chem. Phys.* **7**, 1961–1971 (2007).
41. D. A. Yuen *et al.*, Under the surface: Pressure-induced planetary-scale waves, volcanic lightning, and gaseous clouds caused by the submarine eruption of Hunga Tonga-Hunga Ha'apai volcano. *Earthq. Res. Adv.* **2**, 100134 (2022).
42. C. F. Bohren, D. R. Huffman, *Absorption and Scattering of Light by Small Particles* (Wiley, ed. 1, 1998), 10.1002/9783527618156 (September 23, 2022).
43. B. J. Sumlin, W. R. Heinson, R. K. Chakrabarty, Retrieving the aerosol complex refractive index using PyMieScatt: A Mie computational package with visualization capabilities. *J. Quant. Spectrosc. Radiat. Transf.* **205**, 127–134 (2018).
44. A. E. Bourassa *et al.*, Tomographic retrievals of Hunga Tonga-Hunga Ha'apai volcanic aerosol. *Geophys. Res. Lett.* **50**, e2022GL101978 (2023).
45. E. Asher, 2022-Asher-etal [dataset]. Atmospheric Composition & Chemical Processes: Measurements. https://csl.noaa.gov/groups/csl6/measurements/data/2022-Asher-etal/. Deposited 24 January 2023.
46. G. Taha, OMPS-NPP L2 LP Aerosol Extinction Vertical Profile swath daily 3slit V2 [dataset]. Goddard Earth Sciences Data and Information Services Center (GES DISC). https://disc.gsfc.nasa.gov/datasets/OMPS_NPP_LP_L2_AER_DAILY_2/summary. Accessed 9 June 2022.
47. A. Lambert, W. Read, N. Livesey, MLS/Aura Level 2 Water Vapor (H2O) Mixing Ratio V004 [dataset]. Goddard Earth Sciences Data and Information Services Center (GES DISC). https://disc.gsfc.nasa.gov/datasets/ML2H2O_004/summary?keywords=aura. Accessed 30 June 2022.
48. E. Asher, elizabethasher/hthhPY. GitHub. https://github.com/elizabethasher/hthhPY. Deposited 24 January 2023.